DOWN-SCALING OF SEBAL DERIVED EVAPOTRANSPIRATION MAPS FROM MODIS (250m) TO LANDSAT (30m) SCALE

Sung-ho Hong[1], Jan M.H. Hendrickx[2] and Brian Borchers[3]

[1]Murray State University, Dept. of Geoscience, Murray, KY 42071
Previously at New Mexico Tech, Dept. of Earth and Environmental Science, Socorro, NM 87801
[2]New Mexico Tech, Dept. of Earth and Environmental Science, Socorro, NM 87801
[3]New Mexico Tech, Dept. of Mathematics, Socorro, NM 87801

ABSTRACT

The major problem with high spatial resolution satellite images from Landsat 7 is that imagery is not available very often (i.e. every 16 days or longer) and the coverage area is relatively small (swath width 185km), while images of lower spatial resolution from MODIS are available daily and one image covers a relatively large area (swath width 2,330km). This paper considers the feasibility of applying various down-scaling methods to combine MODIS and Landsat imagery in order to obtain both high temporal and high spatial resolution. The Surface Energy Balance Algorithm for Land (SEBAL) was used to derive daily evapotranspiration (ET) distributions from Landsat 7 and MODIS images. Two down-scaling procedures were evaluated: input down-scaling and output down-scaling. In each down-scaling scheme, disaggregated imagery was obtained by two different processes: subtraction and regression. The primary objective of this study was to investigate the effect of the different down-scaling schemes on the spatial distribution of SEBAL derived ET. We found that all of the four proposed down-scaling methodologies can generate reasonable spatial patterns of the disaggregated ET map. The results

of this study show that output down-scaling with regression between images is the most preferred scheme and input down-scaling with subtraction is the least preferred scheme.

1. INTRODUCTION

Routine monitoring of surface conditions with high spatial resolution satellite data is difficult due to the long return period between successive satellite overpasses. Although the temporal resolution of Landsat is 16 days, even in arid regions only monthly coverage is a reasonable expectation for the availability of clear high-resolution satellite images due to periodic cloud cover (Moran et al., 1996). High-temporal resolution (daily or more frequent) but coarser spatial resolution satellite data including Moderate Resolution Imaging Spectroradiometer (MODIS), Advanced Very High Resolution Radiometer (AVHRR) and Geostationary Orbiting Environmental Satellite (GOES) have therefore been used to conduct routine ET monitoring (e.g. Seguin et al., 1991; e.g. Mecikalski et al., 1999). Coarse resolution images like MODIS provide very useful opportunities to monitor the surface conditions at meso-scale with a temporal resolution of one day. Therefore, down-scaling from MODIS to Landsat scale is a very useful technique to combine the advantages of high temporal and spatial resolutions.

Down-scaling is defined as an increase in spatial resolution following disaggregation of the original data set (Bierkens et al., 2000; Liang, 2004). The process of down-scaling accomplishes a restoration of the variation at a specific scale by assuming that the values of the larger scale are the average of the values at the finer scale and that more uncertainties exist in down-scaled products than up-scaled products because infinitely many down-scaled products are possible (Bierkens et al., 2000). Down-scaling is generally required for the use of available information at a desired fine resolution (Price et al., 2000; Maayar and Chen, 2006). In the last decade, many studies have examined the effects of spatial resolution on surface characteristic representation, but information on down-scaling is limited since most studies have examined up-scaling procedures only (Nellis and Briggs, 1989; Turner et al., 1989; Lam and Quattrochi, 1992; Stoms, 1992; Brown et al., 1993; Vieux, 1993; De Cola, 1994; Mark and Aronson, 1994; Wolock and Price, 1994; Zhang and Montgomery, 1994; Bian et al., 1999; Hong et al., 2009).

Traditionally, down-scaling procedures have been tested in the fields of meteorology and climatology to obtain local climatological information from coarse-resolution remote sensing imagery, but only a few studies have applied disaggregation schemes to surface parameters to increase resolution (Liang, 2004). Most previous research regarding down-scaling using remote sensing imagery has focused on attempting to disaggregate the land cover information. Among the most popular techniques for disaggregation of land cover are artificial neural networks (Kanellopoulos et al., 1992; Atkinson and Tatnall, 1997), mixture modeling (Settle and Drake, 1993; Kerdiles and Grondona, 1996), and supervised fuzzy c-means classification (Bezdek et al., 1984; Foody and Cox, 1994). These techniques have been successfully applied to estimate the proportions of specific classes that occur within each pixel. While this disaggregation information expressed land cover composition, it did not provide any indication of spatial location within the pixel. Atkinson (1997) proposed an idea for an alternative method called "sub-pixel mapping". The proposed technique aimed to determine where the relative proportions of each class are most likely to occur.

More recently, an algorithm for sharpening thermal imagery algorithm called DisTrad was introduced by Kustas et al. (2003). DisTrad sharpens thermal band data to that of the visible and near-infrared bands by using the relationship between radiometric surface temperature (T_{rad}) and the Normalized Difference Vegetation Index (NDVI). The DisTrad technique is based on fitting a second order polynomial between T_{rad} and the aggregated NDVI to the resolution of T_{rad}. Disaggregated sensible heat flux fields estimated by the DisTrad technique using Landsat 7 imagery agreed with ground measured fluxes to within 10 % (Anderson et al., 2004). Most of the very-fine resolution (< 5 m) satellites like IKONOS and Quickbird have visible and near-infrared bands but do not have thermal bands. DisTrad can generate IKONOS resolution thermal imagery with additional information.

In this study, high quality Landsat 7 and Terra MODIS images (Figure 1) were selected to test various down-scaling procedures. Disaggregated daily ET rates from MODIS imagery were compared with the ET rates derived from Landsat imagery. SEBAL estimated daily ETs from Landsat imagery were compared against ground-based eddy covariance measurements in previous research and demonstrated very good agreement (Hendrickx and Hong, 2005; Hong, 2008). The primary objective of this study was to investigate the effect of various relatively simple down-scaling schemes on the spatial distribution of the SEBAL estimated daily ET rate, especially noting how the relative accuracy of ET changes with increasing spatial resolution.

2. METHODS AND MATERIALS

2.1. Study Area and Satellite Imagery

The study area covers a portion of the Middle Rio Grande Valley in New Mexico (Figure 1). The Middle Rio Grande setting is composed of agricultural fields and riparian vegetation. The regional climate is classified as arid/semiarid; its annual precipitation distribution is bimodal, with more than half of the rainfall due to monsoonal patterns in the summer, although the proportion varies considerably from year to year. The average annual air temperature is 15 °C. Summer daily temperatures range from 20 to 40 °C, while winter daily temperatures range from -12 to 10 °C. Mean annual precipitation is about 25 cm and mean annual potential ET is approximately 170 cm. (Stromberg, 1998; Costigan et al., 2000; Scott et al., 2000; Cleverly et al., 2002; Elmore et al., 2002).

Clear-sky Landsat 7 and MODIS images from May 31 and June 16, 2002 were selected for the investigation of the effect of down-scaling processes. Table 1 shows the spectral bands of Landsat 7 and MODIS in the visible, near- to mid-infrared and thermal infrared wavelength regions used for SEBAL application. Both the Landsat data and the MODIS MOD 02 - Level-1B calibrated and geolocated at-aperture radiances have not been corrected for atmospheric conditions since no ground measurements were available to do so and –more importantly– the internal calibration of the sensible heat computation within SEBAL eliminates the need for refined atmospheric correction of surface temperature and reflectance albedo measurements using radiative transfer models (Allen et al., 2007; Bastiaanssen et al., 2005). Since MODIS images are already accurately georeferenced unlike Landsat images, two Landsat images used in this study were georeferenced to closely match each other as well as the MODIS images. This was done by identifying several accurate Ground Control Points (e.g. road intersections and agricultural field boundaries) on the Landsat images and aligning them to fit on the images. The images used in this study covered an 18km x 90km area of the Middle Rio Grande Basin [upper left corner (long/lat): (106°49'W/35°14'N); lower right corner (long/lat): (106°36'W/34°25'N)] approximately from the city of Albuquerque to the Sevilleta LTER (Figure 1).

2.2. Surface Energy Balance Algorithm for Land (SEBAL)

We have selected SEBAL to estimate ET distributions in the Rio Grande Basin for the following reasons: (1) SEBAL consists of physically-based image analysis algorithms using standard satellites imagery and requires a minimum of ancillary meteorological information from surface measurements or atmospheric models. (2) SEBAL deals with a large number of environmental variables and does not assume variables to be constant over space as do many other methods. For example, some methods assume all variables besides surface and air temperatures are spatially constant (Seguin and Itier, 1983; Jackson et al., 1996). (3) In SEBAL the need for atmospheric correction of short-wave and thermal information in images is reduced (Tasumi, 2003), since SEBAL ET estimates depend only on radiometric temperature differences in the scene rather than on the absolute value of the surface temperature. (4) SEBAL has not only been used successfully with Landsat images at spatial scales of 30 – 60m, but also with AVHRR (Advanced Very High Resolution Radiometer) and MODIS (Moderate Resolution Imaging Spectroradiometer) images at spatial scales of 250 – 1000m (Bastiaanssen et al., 2002; Hong et al., 2005; Hafeez et al., 2006). (5) Recent studies with SEBAL in the heterogeneous arid riparian and desert areas of the southwestern US have been successful using Landsat and MODIS images (Fleming et al., 2005; Hendrickx and Hong, 2005; Hong et al., 2005).

SEBAL is a remote sensing flux algorithm that solves the surface energy balance on an instantaneous time scale and for every pixel of a satellite image (Bastiaanssen et al., 2005; Hendrickx and Hong, 2005; Allen et al., 2007b; Hong, 2008). The method is based on the computation of surface albedo (α), surface temperature (T_s), and NDVI from multi-spectral satellite data. The α was calculated from visible to mid-infrared bands (Landsat 7: bands 1 – 5 and 7; MODIS: bands 1 – 4, 6 and 7); the T_s from visible, near-infrared and thermal-infrared bands (Landsat 7: band 3, 4 and 6; MODIS: bands 1, 2, 31 and 32); the NDVI from visible and near-infrared bands (Landsat 7: bands 3 and 4; MODIS: bands 1 and 2). Note that SEBAL also uses 250m and 30m resolution of visible and near-infrared from MODIS and Landsat 7, respectively, to calculate T_s and α. Therefore, the spatial resolution of NDVI, T_s and α estimates in this study are all the same.

The α was used to calculate net short wave radiation, and T_s was used for the calculation of net long wave radiation, soil heat flux and sensible heat flux for each pixel. The NDVI governs the soil heat flux by incorporating light interception effects by canopies and was used to express spatial variability in the aerodynamic roughness of the landscape. The surface slope and aspect of the study area were calculated from a digital elevation model (DEM) of 30 and 250m resolutions. The latent heat flux was computed as the residue of the surface energy balance.

$$LE = R_n - G - H \qquad [1]$$

where R_n is the net radiation flux density [Wm^{-2}], G is the soil heat flux density [Wm^{-2}], H is the sensible heat flux density [Wm^{-2}] and LE (= λET) is the latent heat flux density [Wm^{-2}], which can be converted to the ET rate [mms^{-1}] at the time of satellite passover using the latent heat of vaporization of water λ [Jkg^{-1}].

The SEBAL approach has demonstrated a high accuracy for evaporation mapping worldwide with typical accuracies of about ±15% and ±5% for, respectively, daily and seasonal evaporation estimates (Bastiaanssen et al., 2005; Hendrickx and Hong, 2005). Validation of SEBAL evaporation in Idaho using precision lysimeter measurements (considered the best standard) has shown SEBAL evaporation estimates to be within ±10% at the sub-field scale for daily, monthly and annual time scales (Morse et al., 2000; Allen et al., 2003; Allen et al., 2007a). For more details of the SEBAL algorithm, the reader is referred to the papers (Bastiaanssen et al., 1998; Hendrickx and Hong, 2005; Allen et al., 2007b; Hong, 2008).

2.3. Down-Scaling (disaggregation) Process

Image down-scaling or disaggregation consists of using information taken at larger scales to derive processes at smaller scales. The total number of pixels increases and each output pixel represents a smaller area. Prior to applying the down-scaling procedures suggested in this study, we prepared maps of α, NDVI, T_s and daily ET from Landsat 7 and MODIS images on June 16, 2002 and May 31, 2002 (Figure 2).

In this study, we have disaggregated MODIS scale (250m) imagery to Landsat scale (30m) imagery using four different down-scaling methods (Table 2 and Figure 3). The "input down-scaling" consists of disaggregating MODIS-scale pixels of α, NDVI, and T_s values to obtain pixels at the Landsat-scale prior to applying SEBAL to estimate daily ET. Note that although the SEBAL ET is a nonlinear function of theses inputs, the input down-scaling scheme implicitly assumes linearity. As we shall see later, the nonlinearity does not seem to cause problems in practice. The "output down-scaling" scheme required running SEBAL first and then disaggregated SEBAL estimated daily ET from MODIS to Landsat pixel scale.

Two different disaggregation schemes, subtraction and regression are used in this study (Figure 3). The subtraction method disaggregated imagery by applying the distribution of pixel by pixel difference between two MODIS products to previous or subsequent Landsat images covering the same area. The fine-scale variability within a MODIS pixel is assumed unchanged during the time interval (16 days or longer) between two high quality Landsat images.

For example, in order to disaggregate ET imagery obtained from MODIS imagery of June 16, 2002 with output down-scaling with subtraction (ID #1 in Table 2), first the pixel-by-pixel difference map between MODIS ET on June 16, 2002 and May 31, 2002 was calculated. Second, the calculated difference was added to prior Landsat ET imagery on May 31, 2002 to predict disaggregated ET imagery on June 16, 2002.

The regression method disaggregated imagery by applying linear regression between two MODIS products to the previous or subsequent Landsat product. In this application of output down-scaling with regression, a 1^{st} order linear regression between two ET maps was first calculated, and then the regression was applied to the ET map derived from the prior Landsat image of May 31, 2002 to predict the disaggregated imagery on June 16, 2002. The 1^{st} order regression line was not constrained to zero intercept in order not to change the meaning of the regression coefficients. The regression method used in the study has an assumption that the linear relationship between coarse resolution images is valid between fine-scale resolution imagery and that the fine-scale variability of the area of interest changes linearly during the time interval between two satellite-estimated maps.

The spatial distribution and statistical features of the disaggregated ET maps generated by four different down-scaling schemes were compared with each other. The down-scaled ET maps were also evaluated against the ET map directly derived from Landsat imagery. The performance of the different down-scaling schemes was examined by inspection of: (1) the spatial distribution of disaggregated imagery by each down-scaling scheme to evaluate the changes in spatial pattern after disaggregation and (2) histograms and descriptive statistics of the disaggregated data from each down-scaling scheme. The differences in spatial details between the disaggregated imagery and the original imagery from Landsat were considered. In this study, difference images were created by subtracting the disaggregated pixels from the pixels of the direct Landsat-based estimates ($ET_{down\text{-}scaled} - ET_{Landsat}$). The statistical and spatial characteristics of the differences were evaluated by displaying their spatial distribution and calculating the mean and standard deviation of the absolute differences. Descriptive statistics were calculated based on the absolute value of the difference so that large positive and negative differences would not cancel each other out when the mean difference were calculated.

3. RESULTS AND DISCUSSION

3.1. Landsat and MODIS Imagery Preparation

Landsat- and MODIS-derived α, NDVI, T_s and daily ET distributions on May 31 and June 16 in 2002 are shown in Figures 4 and 5. The area of coverage is 90 x 18km^2 which contains 3000 x 600 pixels for Landsat scale (30m) and 360 x 72 pixels for MODIS scale (250m). The histogram and descriptive statistics including mean and standard deviation (Std) of SEBAL estimates are also shown in Figures 4 and 5. In order to show the spatial distribution in detail, an enlarged area of 6 x 9 km^2 in the Rio Grande riparian area is presented at the bottom of the figures. Linear regressions of Landsat and MODIS scale pixels used in down-scaling with regression method are presented in Figure 6.

3.1.1 Spatial distribution of Landsat- and MODIS-based maps

The frequency distribution and descriptive statistics in Figures 4 and 5 show a wide pixel value range due to the heterogeneous surface covers including riparian vegetation, the Rio Grande River, agricultural fields, bare soil, desert vegetation and urban areas in the study area. Note that a great portion of the pixels (~ 40%) in the study area have close to zero ET rates (0 – 0.5 mmd^{-1}). Lower ET rates correspond to the higher T_s and α and lower NDVI values. In both Landsat and MODIS estimates, the mean values of ET and NDVI of June images were higher but T_s was lower than those from the May images. This indicates that vegetation growth activity (transpiration) increased from the end of May to the middle of June. However, it is difficult to ascertain a significant difference in α values between the two dates.

The full scene of Landsat- and MODIS-based ET, T_s, α and NDVI maps on the same date showed overall similar distributions, but many of the fine details found on the Landsat-based maps have disappeared on the MODIS-based maps. For example, all of the images clearly show that higher ET, low T_s, lower α and higher NDVI occur in the irrigated fields and riparian areas along the Rio Grande Valley, while lower ET, higher T_s and α and lower NDVI values occur in the adjoining desert. The city of Albuquerque has much higher ET rates than the surrounding desert due to the grass and trees in the urban environment. The high spatial resolution of the Landsat-based image resulted in many homogeneous pixels with either high or low ET, T_s, α and NDVI. The low spatial resolution of the MODIS-based map resulted in many mixed pixels consisting partly of high ET, T_s, α and NDVI and partly of low ET, T_s, α and NDVI. The mixed pixels issue is well presented in the NDVI maps. The minimum value of NDVI in the Landsat-based estimate is negative (water pixels) (-0.46 for June 16, 2002 and -0.36 for September 14, 2000), but the MODIS-based NDVI has a positive minimum number. This shows that the 250 x 250 m^2 MODIS pixel size is too big to be composed entirely or mainly of water in our study area.

Also in Figures 4 and 5, the increase in mixed pixels in the MODIS-based maps is clearly presented in the histograms and descriptive statistics. Due to the increase in mixed pixels as spatial resolution increases, MODIS-based ET, T_s, α and NDVI distributions produced a tighter and taller histogram than the one from Landsat imagery. As shown in the table of descriptive statistics, mean values of Landsat and MODIS estimated images are very similar (Figures 4 and 5). However, maps of ET, T_s, α, and NDIV derived from the Landsat 7 image show a greater standard deviation than the maps derived from the MODIS images. The temporal changes in ET, T_s, α and NDVI in the area of agricultural fields along the Rio Grande River are significant between images of 16 days apart. The abrupt changes are clearly shown in Landsat-based maps in the 6 km by 9 km enlarged area. These changes can be detected in the MODIS estimated maps, but are not as clearly represented as they are in the Landsat scale images due to the coarse spatial resolution of the MODIS pixels.

3.1.2. Linear regression between Landsat- and MODIS-based maps

Figure 6 presents the linear regressions of two Landsat and two MODIS estimates, respectively, on May 31, 2002 versus June 16, 2002. The 1:1 line is also drawn in the graphs. Figure 6 was generated in order to answer to the question of whether relationships between ET, T_s, α and NDVI are identical for a MODIS and Landsat image of the same day. The data show a decent agreement in linear regressions between Landsat and MODIS. Therefore, it confirms the feasibility of using the down-scaling methods; especially the regression based ones that are proposed in this study. The regression lines in Figure 6 also support that the ET and NDVI were higher but T_s was lower for the June images than those from May images in both Landsat and MODIS estimates.

3.2. Comparison of Different Down-scaled Maps

Spatial and statistical characteristics of four different down-scaled products at 30m resolution from coarse 250m resolution MODIS-based imagery are presented in Figure 7. The difference maps between MODIS- and Landsat-based ET on June 16, 2002 and between down-scaled daily ET maps versus Landsat-based ET at 30m resolution are shown in Figure 8.

3.2.1. Down-scaling with output subtraction and regression

The mean value of the down-scaled ET map of June in Figure 7 (1) is larger than Landsat-based ET of May (μ: 1.79 mmd^{-1}), and also greater than the mean value of the original

June Landsat-based ET (μ: 1.81 mmd^{-1}). The larger mean values of the down-scaled ET map can be explained by the larger positive pixel-by-pixel difference between the two MODIS-based ET of June and May images than the one between Landsat-based ET images. From Figures 4 and 5, the mean difference between the MODIS-based ET in June and the May MODIS-based ET is calculated as 0.09 mmd^{-1}. This difference is larger than the difference between the original Landsat-based ET of June and May (0.02 mmd^{-1}). Therefore, when these differences between the two MODIS-scale images were added to the Landsat-based ET on May 31, 2002, the down-scaled ET values were higher than the original Landsat-based ET of June 16, 2002. The difference in the SEBAL outcome between Landsat 7 and MODIS is mainly a result of slightly different band widths for each sensor. The band widths of MODIS in the visible and near-infrared, with the exception of Band 3, are narrower than those of Landsat 7. This results in different responses from the surface, which in turn may alter the computed surface α, NDVI and T_s.

The down-scaled map in Figure 7 (2) was produced by applying a linear regression obtained from two MODIS scale images to the Landsat-based ET on May 31, 2002. Therefore, the overall spatial distribution of down-scaled imagery should be similar to the original Landsat-based ET map of May. Compared to Figure 7 (1), Figure 7 (2) shows a smoother pattern (lower standard deviation). This is because regression method does not produce any sharp transitions in the down-scaled image of MODIS scale pixel and is less vulnerable to the georeferencing disparity between Landsat and MODIS images than the subtraction method. In Figure 7 (2), sharp transitions of MODIS scale are easily recognized along the Rio Grande River and also in the lower right side of the enlarged image. Another advantage of regression over subtraction is that a few outliers will hardly affect the linear regression since so many pixels are available for the regression. Most outliers can be caused by georeferencing disagreement among the different satellite images or by abrupt temporal changes between two different dates' images resulting from a rainstorm or irrigation over part of the area.

3.2.2. Input and output down-scaling

The down-scaled ET maps in Figure 7 (3) and 7 (4) were generated after applying SEBAL with down-scaled 30m pixel size of SEBAL input parameters (T_s, α and NDVI) with subtraction and regression method, respectively. The disparity among the down-scaled ET maps between (3) and (4) in Figure 7 is similar to the disparity among the maps in (1) and (2). For example, the maps in Figure 7 (4) are smoother (lower standard deviation) than the maps in Figure (3), because again subtraction method generates a sharp transition and also the georeferencing disagreement between the two MODIS images is smaller than the difference between MODIS and Landsat imagery.

Little differences exist in standard deviation between the maps in Figure 7. However, any difference between input and output down-scaled maps results first from the imperfection of the down-scaling procedure which leads to a disparity between the down-scaled input parameters and the parameters from the original MODIS sensor. Second, the disparity between the input and output down-scaling is also due to the non-linearity of the SEBAL model and the application of different dT-T_s relationships for different pixel size imagery (Hong, 2008). For the input down-scaling $dT = 0.181 \cdot T_s - 54.71$ was used and $dT = 0.209 \cdot T_s - 64.13$ was used for the output down-scaling. That is, because input and output down-scaling used different dT-T_s relationships, the output down-scaled ET imagery must be different from the input down-scaled ET one, even with the linearly related two input data set. Nevertheless, as demonstrated by visual examination of the spatial distribution of ET in Figure 7, the contrast as well as the basic patterns (high and low values and their relative locations) of ET between output down-scaling and input down-scaling show only slight disagreement. The input down-scaling procedure is more complicated than the output down-scaling procedure, since it needs to disaggregate three images compared to one image for output down-scaling. In addition, longer SEBAL processing time is required for input down-scaling because the input images have a higher resolution and a larger file size.

3.3. Limitation of the Proposed Down-scaling Method

The proposed down-scaled method does not always produce reliable results. This section analyzes differences between the down-scaled images and investigates the limitations of the down-scaling schemes.

3.3.1. Difference between down-scaled ET and original Landsat-based ET

Descriptive statistics of the absolute difference of four different down-scaled ET maps against the original Landsat-based ET of June 16, 2002 are shown in Table 3. Descriptive statistics in Table 3 show that mean values of the absolute difference are similar to each other and range from 0.53 to 0.57 mmd^{-1}, but the standard deviation from the regression method is a little lower than from the subtraction method. Table 3 also supports that the difference in down-scaled ET maps between input and output down-scaling schemes was not significant. However, any slight difference between input and output down-scaling can be explained by the difference between the down-scaled input parameters and the original parameters from MODIS imagery.

3.3.2. Georeferencing disagreement among images

Figure 8 shows examples of pixel-by-pixel difference maps between MODIS- and Landsat-based ET and between down-scaled ET and original Landsat-based ET to examine the effect on georeferencing disagreement between images on down-scaling. In general, the satellite image has a georeferencing difference of a size of one or two pixels; therefore, the disparity of the georeferencing accordance between images is easily more than a couple of pixel sizes. Also note that the georeferencing match between images from different satellite sensors is poorer than the ones from same sensors. As shown in Figure 8, the pixel by pixel difference between the MODIS- and Landsat-based ET map shown in (a) has higher standard deviation than the ones in (b) and (c). From the difference in (a), areas with apparently high ET differences (± 2.0 mmd^{-1}) having brown and blue colors are dominantly observed along the boundary between Rio Grande River riparian areas (high ET) and surrounding deserts (low ET). Since the difference maps in (a) were produced by subtracting Landsat-based ET from MODIS-based ET [$ET_{MODIS} - ET_{Landsat}$], the red-colored pixels of the difference maps of (a) represent where the MODIS-based ET is considerably higher than Landsat-based ET. Of course, areas showing blue-colored pixels represent points where the ET from Landsat is considerably higher than the ET from MODIS-based imagery. These extremes are mostly due to pixel size difference or mixed pixels, and disagreement in image georeferencing between Landsat- and MODIS-based imagery.

Dealing with the georeferencing of two maps with spatial resolutions differing by an order of magnitude is not an easy problem. In fact, it was impossible for us to identify accurate common ground control points from both Landsat and MODIS imagery directly because of the huge difference in the spatial resolution. Therefore, it was very difficult to perform georeferencing of two different scale satellite images correctly. The georeferencing difference also appears in histograms. Histograms in Figure 8 indicate that the frequency of almost zero ET difference pixels of (a: 32.4%) is less than the frequency in (b: 39.7 and c: 42.0%). In addition, since georeferencing disagreement between Landsat and MODIS is also embedded in down-scaling with subtraction, the map of (b) in Figure 8 also shows significant differences along the area between riparian and desert areas. These large differences did not appear in Figure 8 (c). This indicates that the georeferencing disagreement between the two Landsat images on June and May is quite small.

3.3.3. Areas having dynamic temporal changes

As mentioned earlier, the subtraction method assumes that fine-scale variability within one MODIS scale pixel is unchanged during the time interval between previous and subsequent imagery. To examine the fine-scale variability in the time interval between previous and subsequent fine-resolution imagery, the spatial distribution of Landsat-based ET on May 31, 2002 and June 16, 2002 was examined. No precipitation was recorded during this 16 day period. Three different land use types including riparian, desert, and agricultural field are shown in the area of 1000m by 1000m (Figure 9). As shown in Figure 9, the spatial variability of daily ET in riparian and desert areas is almost consistent over the 16 day interval. However, agricultural fields show dynamic changes in daily ET over the 16 days due to irrigation or other agricultural activities. Therefore, although the subtraction method may produce a reliable down-scaled image in less dynamic (for example, no localized rainfall event) areas such as riparian and desert environments; it is impossible to precisely predict down-scaled imagery in areas experiencing dynamic changes such as agricultural fields.

The method of down-scaling with regression method is dependent upon the regression slope and intercept between two MODIS-based images. The regressions in Figure 6 do not allow abrupt changes (greater than 20%) in ET and other surface parameter between May 31 and June 16. Therefore, the regression method has limitations in areas experiencing a dynamic temporal change in a short period of time.

4. CONCLUSIONS

Despite encountering some issues, this study has shown that all of the proposed down-scaling methodologies could be used to predict reasonable spatial patterns of daily ET within each coarse MODIS scale pixel over the Middle Rio Grande Basin. This study also indicates that down-scaled ET values from coarse resolution remotely sensed data are not always reliable. In particular, the area of interest for image disaggregation needs to be in less temporally dynamic conditions at the coarse MODIS scale in order to produce reliable results.

Georeferencing disagreement between Landsat and MODIS images is the most significant issue for the application of the down-scaling schemes suggested in this study. Based on our results, the regression method is less vulnerable to this georeferencing disagreement between different satellite images than the subtraction method; therefore regression produces more reliable results than subtraction. We also found that the differences in down-scaled ET maps between input and output down-scaling schemes were not significant. However, since the input down-scaling procedure is more complicated and requires longer SEBAL processing time than output down-scaling, we recommend output down-scaling over input down-scaling. Therefore, we conclude that output down-scaling with regression is the most preferred scheme among the four proposed down-scaling schemes. The least preferred scheme is input down-scaling with subtraction.

ACKNOWLEDGEMENT

This study was sponsored by NASA Cooperative Agreement NNA06CN01A.

REFERENCES

Allen, R.G., A. Morse, and M. Tasumi. 2003. Application of SEBAL for western US water rights regulation and planning Proceedings of the International Workshop on Remote Sensing of Crop Evapotranspiration for Large Regions. 54th IEC Meeting of the International Commission on Irrigation and Drainage (ICID), Montpellier, France.

Allen, R.G., M. Tasumi, A. Morse, R. Trezza, J.L. Wright, W. Bastiaanssen, W. Kramber, I. Lorite, and C.W. Robison. 2007a. Satellite-based Energy Balance for Mapping Evapotranspiration with Internalized Calibration (METRIC) – Applications. Journal of Irrigation and Drainage Engineering 133:395-406.

Allen, R.G., M. Tasumi, and R. Trezza. 2007b. Satellite-based Energy Balance for Mapping Evapotranspiration with Internalized Calibration (METRIC) – Model. Journal of Irrigation and Drainage Engineering 133:380-394.

Anderson, M.C., J.M. Norman, J.R. Mecikalski, R.D. Torn, W.P. Kustas, and J.B. Basara. 2004. A multiscale remote sensing model for disaggregating regional fluxes to micrometeorological scales. Journal of Hydrometeorology 5:343-363.

Atkinson, P.M., and A.R.L. Tatnall. 1997. Neural networks in remote sensing. International Journal of Remote Sensing 18:699-709.

Bastiaanssen, W.G.M., M. Menenti, R.A. Feddes, and A.A.M. Holtslag. 1998. A remote sensing surface energy balance algorithm for land (SEBAL). Part 1: Formulation. Journal of Hydrology 212-213:198-212.

Bastiaanssen, W.G.M., M.D. Ahmad, and Y. Chemin. 2002. Satellite surveillance of evaporative depletion across the Indus Basin. Water Resources Research 38:1273-1281.

Bastiaanssen, W.G.M., E.J.M. Noordman, H. Pelgrum, G. Davids, B.P. Thoreson, and R.G. Allen. 2005. SEBAL model with remotely sensed data to improve water-resources management under actual field conditions. Journal of Irrigation and Drainage Engineering 131:85-93.

Bezdek, J.C., R. Ehrlich, and W. Full. 1984. FCM: the fuzzy c-means clustering algorithm. Computers and Geosciences 10:191-203.

Bian, L., R. Butler, D.A. Quattrochi, and P.M. Atkinson. 1999. Comparing effects of aggregation methods on statistical and spatial properties of simulated spatial data. Photogrammetry and Remote Sensing 65:73-84.

Bierkens, M.F.P., P.A. Finke, and D.E. Willigen. 2000. Upscaling and downscaling methods for environmental research. Wageningen University and Research Centre, Kluwer Academic Publishers.

Brown, D.G., L. Bian, and S.J. Walsh. 1993. Response of a distributed watershed erosion model to variations in input data aggregation levels. Computers and Geosciences 19:499-509.

Carrion, D., M. Gianinetto, and M. Scaioni. 2002. GEOREF: a Software for Improving the Use of Remote Sensing Images in Environmental Applications. In Proc. of IEMSS 2002 Int. Meeting, 24-27 June, Lugano, Switzerland:360-366.

Cleverly, J.R., C.N. Dahm, J.R. Thibault, D.J. Gilroy, and J.E.A. Coonrod. 2002. Seasonal estimates of actual evapotranspiration from Tamarix ramosissima stands using 3-dimensional eddy covariance. Journal of Arid Environments 52:181-197.

Costigan, K.R., J.E. Bossert, and D.L. Langley. 2000. Atmospheric/hydrologic models for the Rio Grande Basin: simulations of precipitation variability. Global and Planetary Change 25:83-110.

De Cola, L. 1994. Simulating and mapping spatial complexity using multi-scale techniques. International Journal of Geographical Information Systems 8:411-427.

Elmore, A.J., J.F. Mustard, and S.J. Manning. 2002. Regional patterns of plant community response to changes in water: Owens Valley, California. Ecological Applications 13:443-460.

Eugenio, F., and F. Marqués. 2003. Automatic Satellite Image Georeferencing Using a Contour-Matching Approach. IEEE Transactions on Geoscience and Remote Sensing 41:2869-2880.

Fleming, K., J.M.H. Hendrickx, and S.-H. Hong. 2005. Regional mapping of root zone soil moisture using optical satellite imagery. Proceedings of International Society for Optical Engineering, SPIE 5811:159-170.

Foody, G.M., and D.P. Cox. 1994. Sub-pixel land cover composition estimation using a linear mixture model and fuzzy membership functions. International Journal of Remote Sensing 15:619-631.

Hafeez, M., M. Andreini, J. Liebe, J. Friesen, A. Marx, and N.v.d. Giesen. 2006. Hydrological parameterization through remote sensing in Volta Basin, West Africa. International Journal of River Basin Management 4:1-8.

Hendrickx, J.M.H., and S.-H. Hong. 2005. Mapping sensible and latent heat fluxes in arid areas using optical imagery. Proceedings of International Society for Optical Engineering, SPIE 5811:138-146.

Hong, S.-H., J.M.H. Hendrickx, and B. Borchers. 2005. Effect of scaling transfer between evapotranspiration maps derived from LandSat 7 and MODIS images. Proceedings of International Society for Optical Engineering, SPIE 5811:147-158.

Hong, S.-H. 2008. Mapping regional distributions of energy balance components using optical remotely sensed imagery. PhD. Thesis. Hydrology Program, New Mexico Tech.

Hong, S.-H., J.M.H. Hendrickx, and B. Borchers. 2009. Up-scaling of SEBAL derived evapotranspiration maps from Landsat (30 m) to MODIS (250 m) scale Journal of Hydrology 370:122-138.

Jackson, T.J., J. Schmugge, and E.T. Engman. 1996. Remote sensing applications to hydrology: soil moisture. Hydrological Sciences Journal 41:517-530.

Justice, C.O., A. Belward, J. Morisette, P. Lewis, J. Privette, and F. Baret. 2000. Developments in the ‘validation’ of satellite sensor products for the study of the land surface. International Journal of Remote Sensing 21:3383–3390.

Kanellopoulos, I., A. Varfis, G.G. Wilkinson, and J. Megier. 1992. Land cover discrimination in SPOT HRV imagery using an artificial neural network: a 20 class experiment. International Journal of Remote Sensing 13:917-924.

Kerdiles, H., and M.O. Grondona. 1996. NOAA-AVHRR NDVI decomposition and subpixel classification using linear mixing in the Argentinean Pampa. International Journal of Remote Sensing 16:1303-1325.

Kustas, W.P., J.M. Norman, M.C. Anderson, and A.N. French. 2003. Estimating subpixel surface temperatures and energy fluxes form the vegetation index-radiometric temperature relationship. Remote Sensing of Environment 85:429-440.

Lam, N., and D.A. Quattrochi. 1992. On the issues of scale, resolution, and fractal analysis in the mapping sciences. Professional Geographer 44:88-98.

Liang, S. 2004. Quantitative Remote Sensing of Land Surfaces John Wiley and Sons, Inc.

Ma, Y., J. Wang, R. Huang, G. Wei, M. Menenti, Z. Su, Z. Hu, F. Gao, and J. Wen. 2003. Remote sensing parameterization of land surface heat fluxes over arid and semi-arid areas. Advances in Atmospheric Sciences 20:530-539.

Maayar, M.E., and J.M. Chen. 2006. Spatial scaling of evapotranspiration as affected by heterogeneities in vegetation, topography, and soil texture. Remote Sensing of Environment 102:33-51.

Mark, D.M., and P.B. Aronson. 1994. Scale dependent fractal dimensions of topographic surfaces: An empirical investigation with applications in geomorphology and computer mapping. Mathematical Geology 16:671-683.

Mecikalski, J.R., G.R. Diak, M.C. Anderson, and J.M. Norman. 1999. Estimating fluxes on continental scales using remotely-sensed data in an atmospheric-land exchange model. Journal of Applied Meteorology 38:1352-1369.

Moran, M.S., A.F. Rahman, J.C. Washburne, and W.P. Kustas. 1996. Combining the Penman-Monteith equation with measurements of surface temperature and reflectance to estimate evaporation rates of semiarid grassland. Agricultural and Forest Meteorology 80:87-109.

Morse, A., M. Tasumi, R.G. Allen, and W.J. Kramer. 2000. Application of the SEBAL methodology for estimating consumptive use of water and streamflow depletion in the Bear river basin of Idaho through remote sensing. Final report submitted to the Raytheon Systems Company, Earth Observation System Data and Information System Project, by Idaho Department of Water Resources and University of Idaho.

Nellis, M.D., and J.M. Briggs. 1989. The effect of spatial scale on Konza landscape classification using textural analysis. Landscape Ecology 2:93-100.

Price, D.T., D.W. McKennery, I.A. Nalder, M.T. Hutchinson, and J.L. Kesteven. 2000. A comparison of two statistical methods for spatial interpolation of Canadian monthly mean climate data. Agricultural and Forest Meteorology 101:81-94.

Rigo, G., E. Parlow, and D. Oesch. 2006. Validation of satellite observed thermal emission with in-situ measurements over an urban surface. Remote Sensing of Environment 104:201-210.

Schowengerdt, R.A. 1997. Models and methods for image processing. Second edition ed. Academic Press, San Diego.

Scott, R.L., J.W. Shuttleworth, G. D.C., and M.I. T. 2000. The water use of two dominant vegetation communities in a semiarid riparian ecosystem. Agricultural and Forest Meteorology 105:241-256.

Seguin, B., J.-P. Lagouarde, and M. Saranc. 1991. The assessment of regional crop water conditions from meteorological satellite thermal infrared data. Remote Sensing of Environment 35:141-148.

Seguin, B.D., and B. Itier. 1983. Using midday surface temperature to estimate daily evapotranspiration from satellite thermal IR data. International Journal of Remote Sensing 4:371-383.

Settle, J.J., and N.A. Drake. 1993. Linear mixing and the estimation of ground cover proportions. International Journal of Remote Sensing 14:1159-1177.

Stoms, D. 1992. Effects of habitat map generalization in biodiversity assessment. Photogrammetric Engineering and Remote Sensing 58:1587-1591.

Stromberg, J.C. 1998. Dynamics of Fremont cottonwood (Populus fremontii) and saltcedar (Tamarix chinensis) populations along the San Pedro River, Arizona. Journal of Arid Environments 40:133-155.

Tasumi, M. 2003. Progress in operational estimation of regional evapotranspiration using satellite imagery, Ph.D. Thesis, University of Idaho, Moscow, Idaho.

Turner, M.G., R.V. O'Neil, R.H. Gardner, and B.T. Milne. 1989. Effects of changing spatial scale on the analysis of landscape pattern. Landscape Ecology 3:153-162.

Valor, E., and V. Caselles. 1996. Mapping land surface emissivity from NDVI: Application to European, African, and South American areas. Remote Sensing of Environment 57:167-184.

Vieux, B.E. 1993. DEM Aggregation and smoothing effects on surface runoff modeling. Journal of Computing in Civil Engineering 7:310-338.

Wolock, D.M., and C.V. Price. 1994. Effects of digital elevation model map scale and data resolution on a topography-based watershed model. Water Resources Research 40:3041-3052.

Zhang, W., and D.R. Montgomery. 1994. Digital elevation model grid size, landscape representation, and hydrologic simulations. Water Resources Research 30:1019-1028.

Table 1. Band spatial resolutions (m) and wavelengths (μm) of Landsat 7 and MODIS sensors.

Sensors		Band number								
		1	2	3	4	5[#]	6	7	31	32
Landsat 7	Pixel size [m]	30	30	30	30	30	60	30	NA*	NA*
	Band width [μm]	0.45–0.51	0.52–0.60	0.63–0.69	0.75–0.9	1.55–1.75	10.4–12.5	2.09–2.35	NA*	NA
MODIS	Pixel size [m]	250	250	500	500	500	500	500	1000	1000
	Band width [μm]	0.62–0.67	0.84–0.87	0.46–0.48	0.54–0.56	1.23–1.25	1.63–1.65	2.11–2.15	10.8–11.3	11.8–12.3

[#]MODIS band5 is not used in this study because of streaking noise, *Not available

Table 2. Four different down-scaling methods used in this study.

Down-scaling approach	Down-scaling operation	ID	Method
Output (ET)	Subtraction	1	$(MCET_{250} – MPET_{250}) + LPET_{30}$
	Regression	2	Regr*($MPET_{250}$, $MCET_{250}$) to $LPET_{30}$
Input (α, NDVI, T_s)	Subtraction	3	$(MCANT_{250} – MPANT_{250}) + LPANT_{30}$
	Regression	4	Regr($MPANT_{250}$, $MCANT_{250}$) to $LPET_{30}$

*1^{st} order regression, for example Regr(x,y) to z represents applying 1^{st} order regression between x (predictor) and y (response) to z as a predictor.

$LPET_{30}$: 30m resolution ET map from prior (May 31, 2002) Landsat

$LPANT_{30}$: 30m resolution of α, NDVI and T_s maps from prior Landsat

$MCET_{250}$: 250m resolution of ET map from current (June 16, 2002) MODIS

$MPET_{250}$: 250m resolution of ET map from prior (May 31, 2002) MODIS

$MCANT_{250}$: 250m resolution of α, NDVI and T_s maps from current MODIS

$MPANT_{250}$: 250m resolution of α, NDVI and T_s maps from prior MODIS

ET: daily evapotranspiration rate [mmd^{-1}], α: surface albedo [-], NDVI: Normalized Difference Vegetation Index [-], and T_s: surface Temperature [K]

Table 3. Descriptive statistics of the difference [$mm d^{-1}$] of down-scaled ET against original Landsat-based ET of June 16, 2002. (note: mean and standard deviation are calculated from the absolute difference).

Down-scaling approach	Down-scaling operation	ID	Mean absolute difference	Standard deviation
Output	Subtraction	1	0.53	0.72
	Regression	2	0.57	0.70
Input	Subtraction	3	0.55	0.77
	Regression	4	0.54	0.70

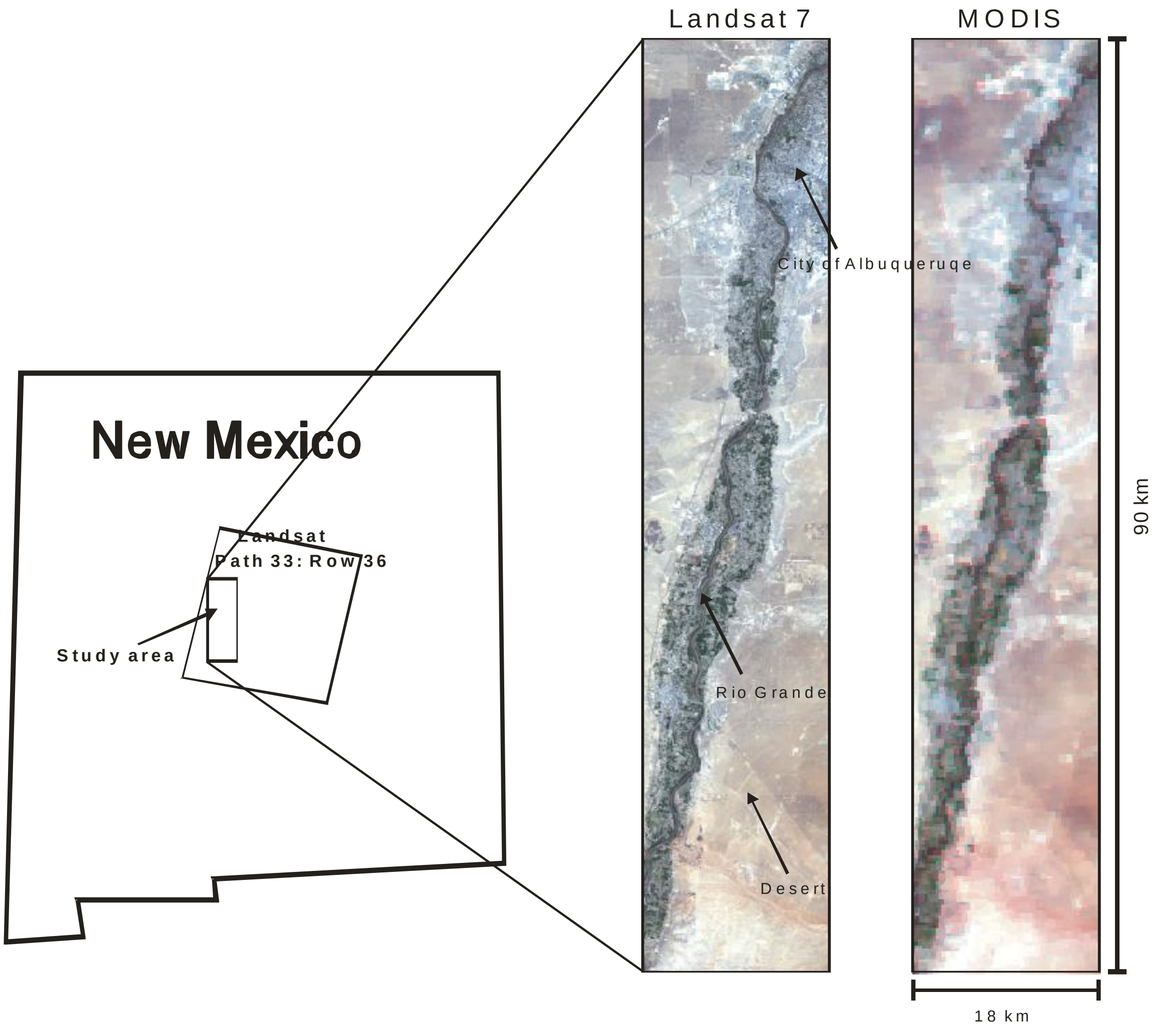

Figure 1. Location of the study area (18km by 90km). True color Landsat 7 (30m by 30m resolution) and MODIS (250m by 250m resolution) images on June 16, 2002.

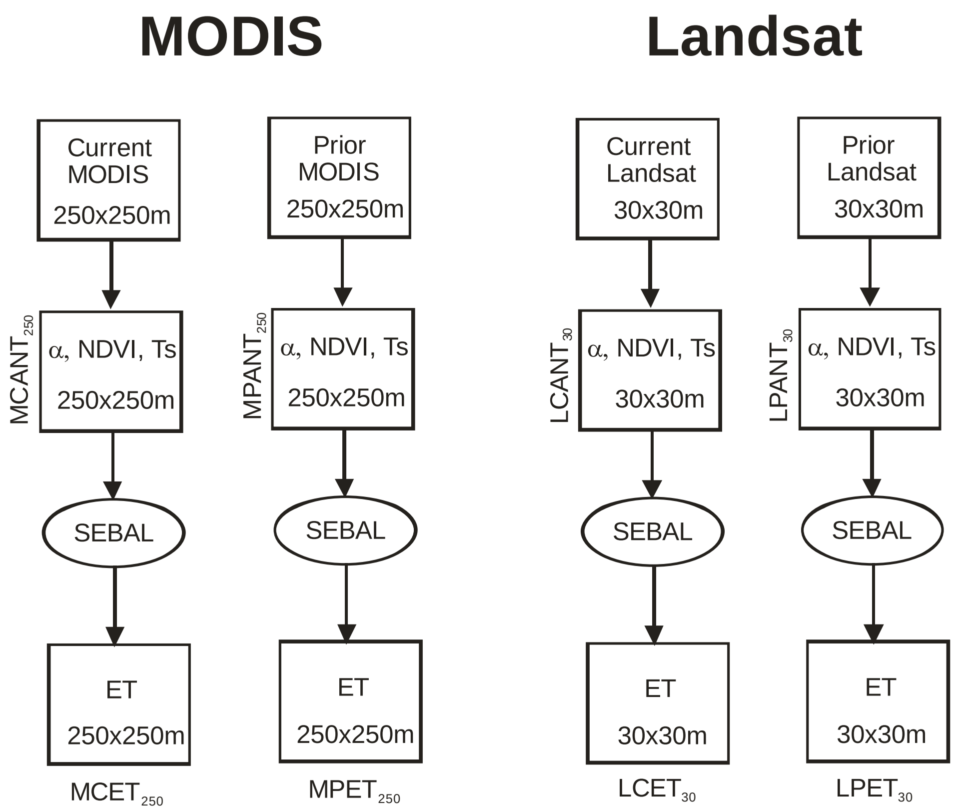

Figure 2. Preprocessing for down-scaling scheme. [$LPET_{30}$: 30m resolution ET map from prior (May 31, 2002) Landsat, $LCET_{30}$: 30m resolution ET map from current (June 16, 2002) Landsat, $LPANT_{30}$: 30m resolution of α, NDVI and T_s maps from prior Landsat, $LCANT_{30}$: 30m resolution of α, NDVI and T_s maps from current Landsat, $MCET_{250}$: 250m resolution of ET map from current MODIS, $MPET_{250}$: 250m resolution of ET map from prior MODIS, $MCANT_{250}$: 250m resolution of α, NDVI and T_s maps from current MODIS, $MPANT_{250}$: 250m resolution of α, NDVI and T_s maps from prior MODIS]

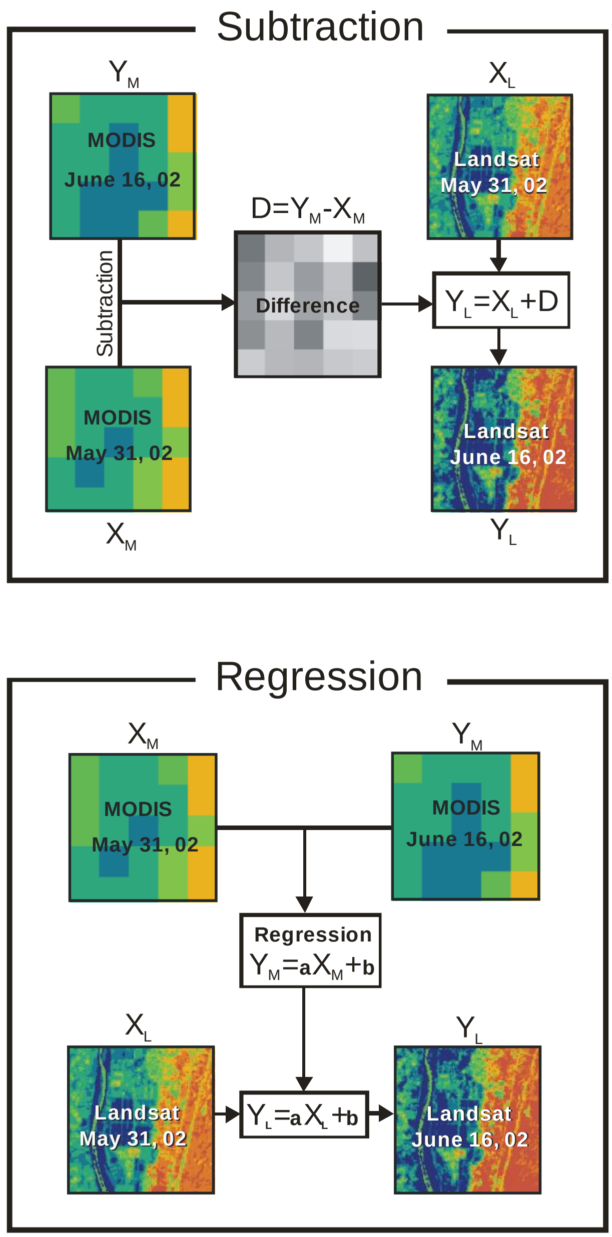

Figure 3. Schematic of two disaggregation methods used in this study.

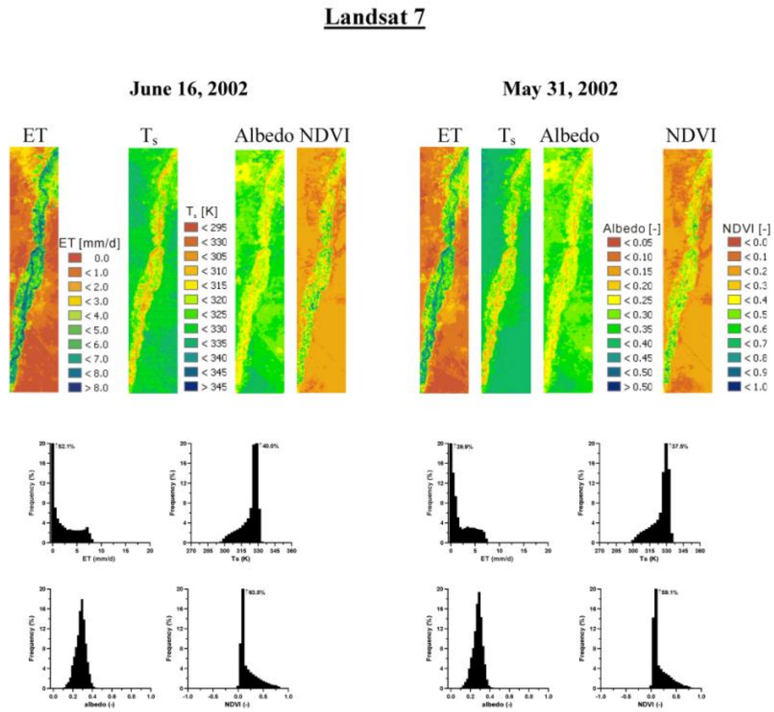

	ET	T_s	α	NDVI		ET	T_s	α	NDVI
Mean	1.81	325.2	0.29	0.18	Mean	1.79	326.8	0.29	0.17
Std	2.46	7.4	0.05	0.15	Std	2.15	7.5	0.05	0.14

Figure 4. SEBAL estimated ET, T_s, α and NDVI from Landsat 7 on June 16, 2002 and May 31, 2002 (30m by 30m resolution). Bin size of the ET, T_s, α and NDVI histogram is 0.5 mmd^{-1}, 2.5 K, 0.02, and 0.05, respectively and frequency occurrence exceeding 20% marked next to the arrow.

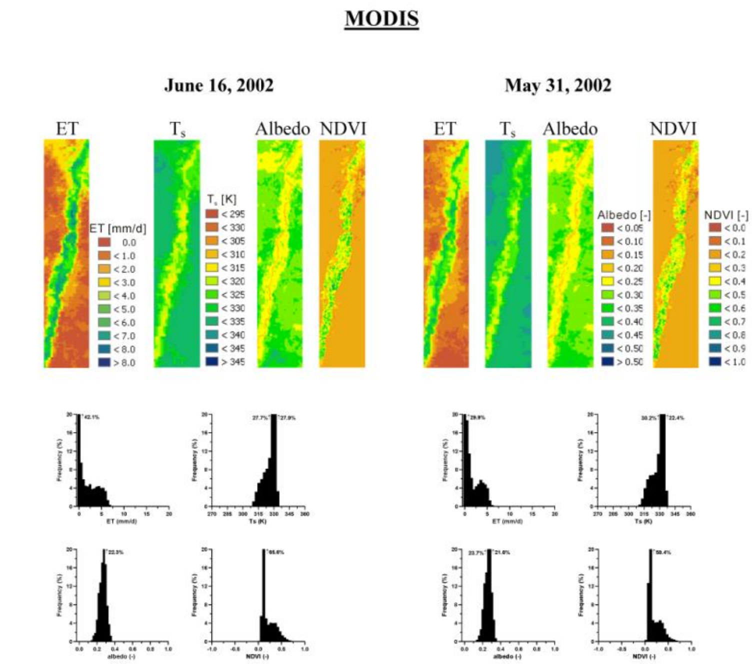

	ET	T_s	α	NDVI
Mean	1.86	327.6	0.28	0.20
Std	2.07	5.5	0.04	0.12

	ET	T_s	α	NDVI
Mean	1.77	329.9	0.27	0.19
Std	1.72	5.8	0.04	0.11

Figure 5. SEBAL estimated ET, T_s, α and NDVI from MODIS on June 16, 2002 and May 31, 2002 (250m by 250m resolution).

Between Landsat estimates on May 31, 2002 and June 16, 2002

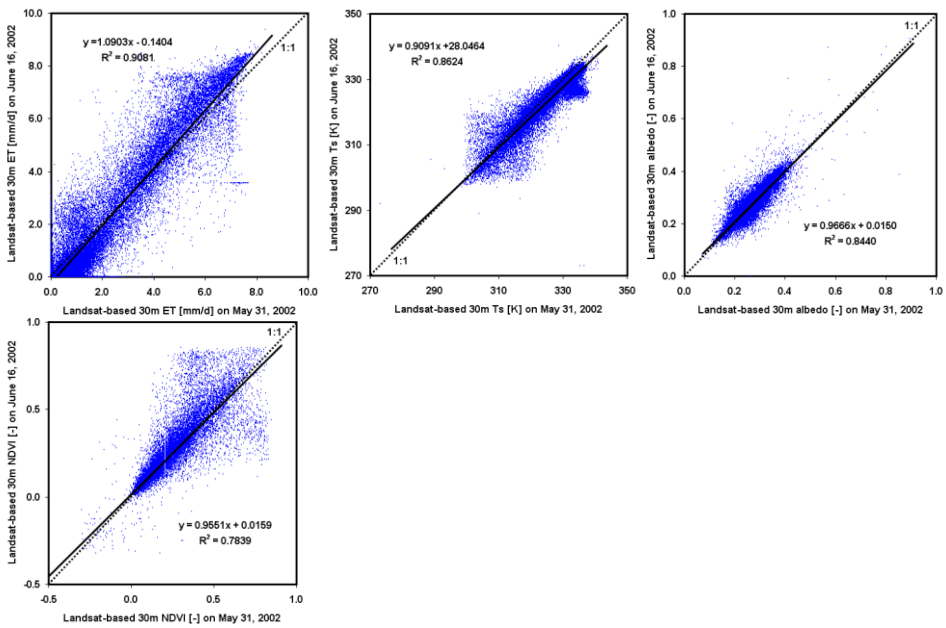

Between MODIS estimates on May 31, 2002 and June 16, 2002

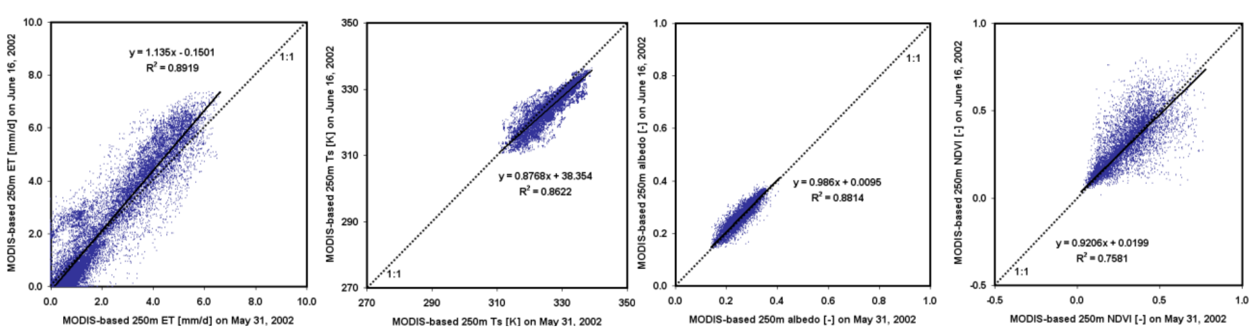

Figure 6. Linear regressions used in down-scaling scheme.

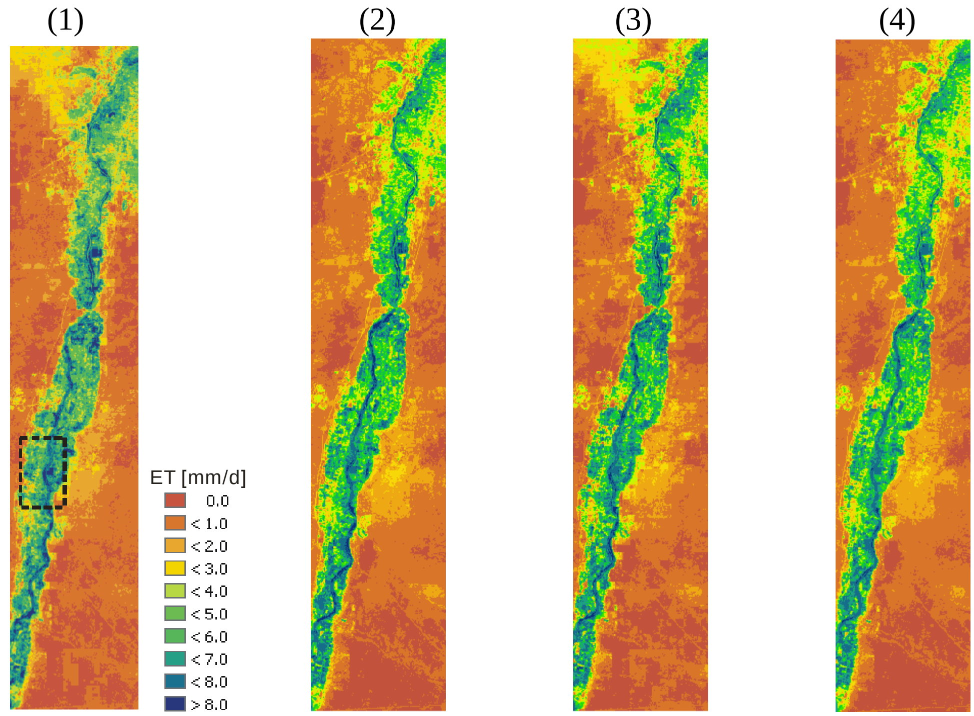

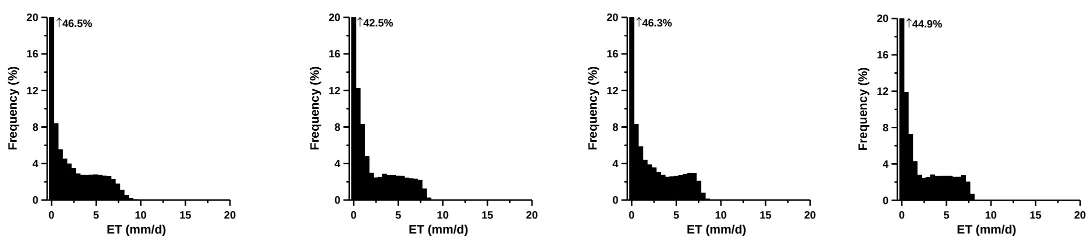

	(1)	(2)	(3)	(4)
Mean	1.94	1.92	1.97	1.85
Std	2.45	2.40	2.47	2.37

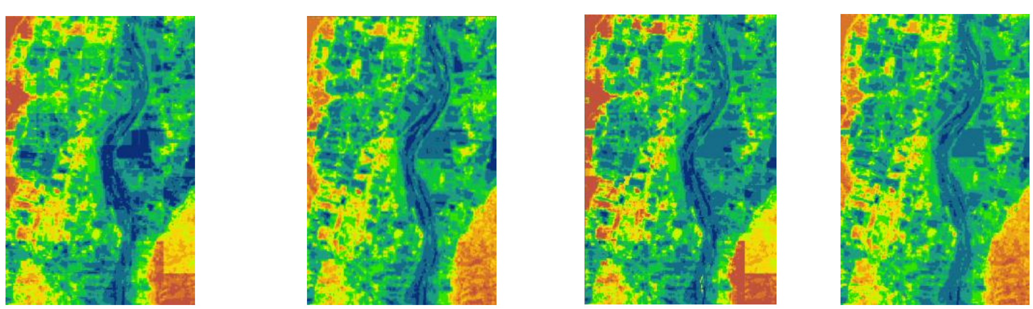

Figure 7. Down-scaled ET map from (1) output with subtraction, (2) output with regression, (3) input with subtraction and (4) input with regression. Bin size of the ET is 0.5 mmd^{-1} and frequency occurrence exceeding 20% marked next to the arrow. Enlarged areas (6 x 9km^2) shown at the bottom correspond to the dotted square of the upper images.

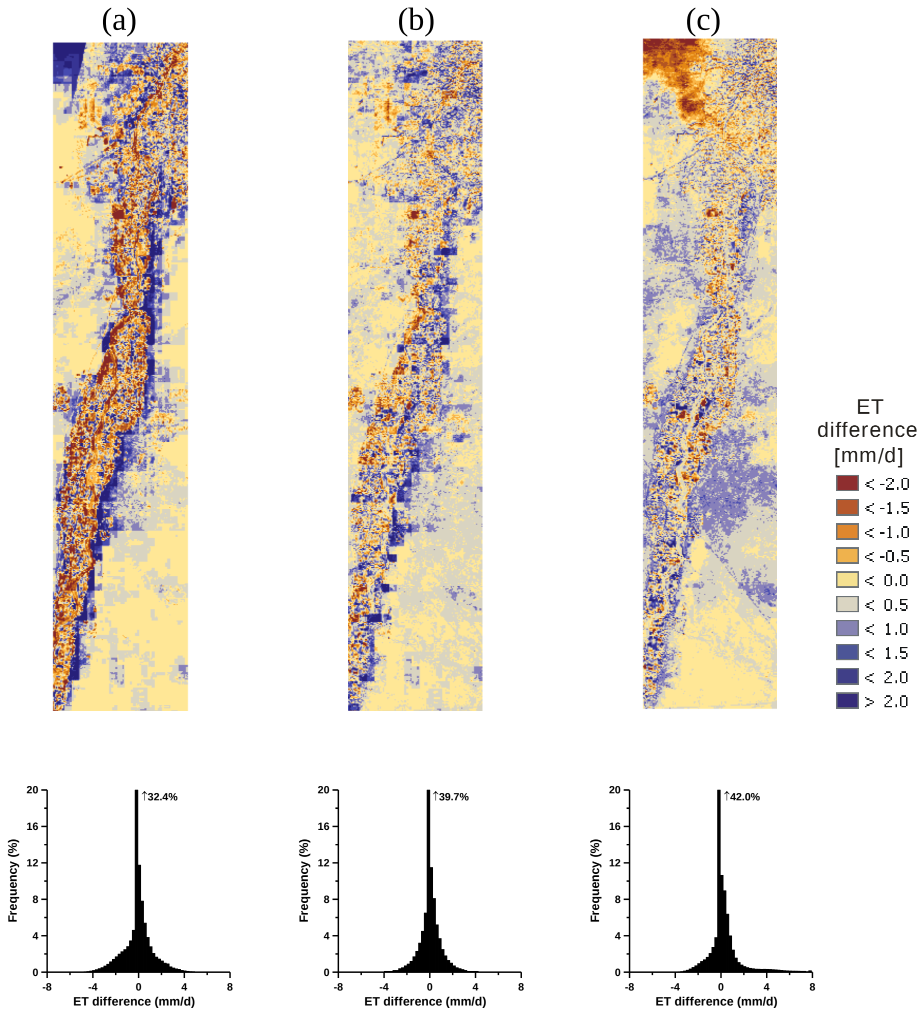

Std	1.20	0.88	0.89

Figure 8. Pixel by pixel difference ET map (a) between MODIS- and Landsat-based ET maps on June 16, 2002, (b) between down-scaled ET (output with subtraction) and Landsat-based ET of June and (c) between down-scaled ET (output with regression) and Landsat-based ET of June. Bin size of the ET difference in the histogram is 0.25 mmd^{-1}.

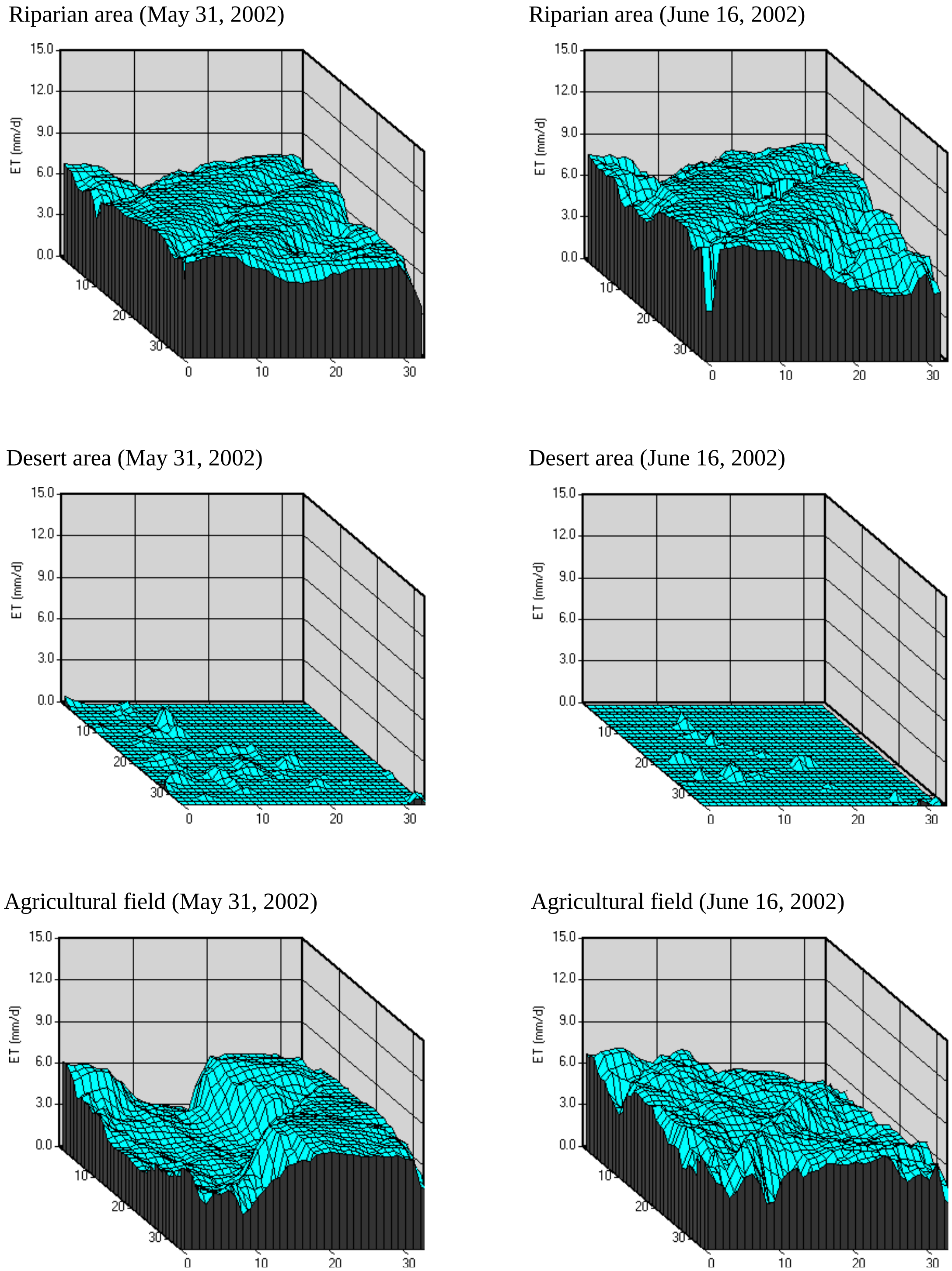

Figure 9. 3-D spatial distribution of Landsat-based ET of different land cover types at 30 x 30m^2 resolution in area of 1000 x1000m^2 on May 31, 2002 and June 16, 2002.